

**Development of bio-composites with novel characteristics:  
Evaluation of phenol-induced antibacterial, biocompatible and  
biodegradable behaviours**

**Dr Hafiz Iqbal<sup>1</sup>  
Dr Godfrey Kyazze<sup>1</sup>  
Dr Ian Locke<sup>1</sup>  
Thierry Tron<sup>2</sup>  
Prof Taj Keshavarz<sup>1</sup>**

<sup>1</sup> Faculty of Science and Technology, University of Westminster, London, UK

<sup>2</sup> Aix Marseille Université, CNRS, Marseille, France

“NOTICE: this is the author’s version of a work that was accepted for publication in *Carbohydrate Polymers*. Changes resulting from the publishing process, such as peer review, editing, corrections, structural formatting, and other quality control mechanisms may not be reflected in this document. Changes may have been made to this work since it was submitted for publication. A definitive version was subsequently published in *Carbohydrate Polymers*, 131 (2015), 197-207, doi:

[10.1016/j.carbpol.2015.05.046](https://doi.org/10.1016/j.carbpol.2015.05.046)”

---

The WestminsterResearch online digital archive at the University of Westminster aims to make the research output of the University available to a wider audience. Copyright and Moral Rights remain with the authors and/or copyright owners.

Users are permitted to download and/or print one copy for non-commercial private study or research. Further distribution and any use of material from within this archive for profit-making enterprises or for commercial gain is strictly forbidden.

---

Whilst further distribution of specific materials from within this archive is forbidden, you may freely distribute the URL of WestminsterResearch: (<http://westminsterresearch.wmin.ac.uk/>).

In case of abuse or copyright appearing without permission e-mail [repository@westminster.ac.uk](mailto:repository@westminster.ac.uk)

1           **Development of bio-composites with novel characteristics: Evaluation of phenol-**  
2                           **induced antibacterial, biocompatible and biodegradable behaviours**

3  
4       Hafiz M. N. Iqbal<sup>a,\*</sup>, Godfrey Kyazze<sup>a</sup>, Ian C. Locke<sup>a</sup>, Thierry Tron<sup>b</sup>, Tajalli Keshavarz<sup>a,\*</sup>

5  
6       <sup>a</sup> Applied Biotechnology Research Group, Department of Life Sciences, Faculty of Science  
7       and Technology, University of Westminster London, W1W 6UW, United Kingdom; <sup>b</sup> Aix-  
8       Marseille Université, CNRS, Centrale Marseille, iSm2 UMR 7313, 13397 Marseille, France.

9       \*Corresponding author Tel.: +44 020 79115030; fax: +44 020 79115087; E-mail addresses:

10       hafiz.iqbal@my.westminster.ac.uk (H.M.N. Iqbal), t.keshavarz@westminster.ac.uk (T.  
11       Keshavarz).

12  
13       **Abstract**

14       This paper describes a laccase-assisted grafting of gallic acid (GA) and thymol (T) as  
15       functional entities onto the previously developed P(3HB)-g-EC composite. GA-g-P(3HB)-g-  
16       EC and T-g-P(3HB)-g-EC bio-composites were prepared by laccase-assisted free radical-  
17       induced graft polymerisation of GA and T onto the P(3HB)-g-EC based composite using  
18       surface dipping and incorporation technique. The results of the antibacterial evaluation for  
19       the prepared composites indicated that 15GA-g-P(3HB)-g-EC, 15T-g-P(3HB)-g-EC and 20T-  
20       g-P(3HB)-g-EC composites possessed the strongest bacteriostatic and bactericidal activities  
21       against Gram-positive *B. subtilis* NCTC 3610 and *S. aureus* NCTC 6571 and Gram-negative  
22       *E. coli* NTCT 10418 and *P. aeruginosa* NCTC 10662 strains. In this study, we have also  
23       tested GA-g-P(3HB)-g-EC and T-g-P(3HB)-g-EC bio-composites for their ability to support  
24       and maintain multilineage differentiation of human keratinocyte-like (HaCaT) skin cells *in-*  
25       *vitro*. From the cytotoxicity results, the tested composites showed 100% viability and did not

26 induce any adverse effect on a HaCaT's morphology. Finally, in soil burial evaluation, a  
27 progressive increase in the degradation rate of GA-g-P(3HB)-g-EC and T-g-P(3HB)-g-EC  
28 bio-composites was recorded with the passage of time up to 6 weeks. In summary, our  
29 current findings suggest that GA-g-P(3HB)-g-EC and T-g-P(3HB)-g-EC bio-composites are  
30 promising candidates for biomedical type applications such as skin regeneration, multiphasic  
31 tissue engineering and/or medical implants.

32

33 **Keywords:** Laccase; Bio-composite, Gallic acid; Thymol; Antibacterial; HaCaT compatible

34

### 35 **1. Introduction**

36 In recent years, with the increasing emergence of infectious diseases caused by various  
37 microorganisms, there is an urgent need for the development of non-toxic green polymeric  
38 materials and/or composites with antimicrobial activity. Laccase-assisted grafting has  
39 recently been the focus of green chemistry technologies in response to the growing  
40 environmental concerns, legal restrictions and advances in science. In principle, laccase-  
41 assisted grafting may modify and/or impart a variety of new functionalities to the materials of  
42 interest as the modified materials through grafting have boundless applications (Božič et al.,  
43 2012; Iqbal et al., 2014a).

44 In recent years, with increasing consciousness to reduce, and preferably eradicate a bacterial  
45 population in healthcare facilities and possibly to cut pathogenic infections, development of  
46 materials with novel characteristics are considered with urgency. The antibacterial features of  
47 silver nanoparticles have been reported, however, excess release of silver nanoparticles  
48 inhibits osteoblasts growth and consequently can also cause many severe side effects such as  
49 cytotoxicity (Sandukas et al., 201; Albers et al., 2013; Wang et al., 2014). In this context,

50 there is a need for green composites with antimicrobial activity to reduce or even eliminate  
51 the risk of bacterial infection without cytotoxicity.

52 Antimicrobial products may be fabricated by introducing antimicrobial agents through  
53 surface coating or dipping, spraying or incorporating microbicidal functional groups with  
54 cellulose (Dong et al., 2014). However, in practice, the main drawback of the various  
55 physical/chemical methods is the risk of premature delamination and short-term antibacterial  
56 effects (Hiriart-Ramírez et al., 2012). On the other hand, laccase-assisted grafting and  
57 incorporation of microbicidal groups, such as natural phenols seems to be a promising  
58 technique. This technique offers clean and safe alternative to the currently practiced  
59 physical/chemical methods (Chen et al., 2000; Aljawish et al., 2012). In the production of  
60 functional materials, enzyme specificity may offer the potential to better control the polymer  
61 function through precise modifications in the polymer structure (Chen et al., 2000; Yamada et  
62 al., 2000; Iqbal et al., 2014b,c).

63 It is well-known that phenols are typical laccase substrates because their redox potentials are  
64 low enough to allow electron abstraction by Cu<sup>I</sup> reaction site of the laccase. They are  
65 oxidized into phenoxy radicals which, depending on the reaction conditions, can  
66 spontaneously polymerize via radical coupling, or rearrange themselves into highly-reactive  
67 quinones through a disproportionation mechanism. Figure 1 illustrates a schematic mechanism  
68 for laccase action in the preparation of phenol grafted P(3HB)-*g*-EC composites. Among the  
69 tested phenolic structures GA and T, both have pronounced antibacterial features toward a  
70 wide spectrum of Gram-positive and Gram-negative bacteria. In addition, their flavouring,  
71 antioxidant and antiseptic characteristics has already been reported elsewhere by several  
72 authors (Sanchez-Garcia et al. 2008; Archana et al. 2011; Rukmani and Sundrarajan 2012;  
73 Shahidi et al., 2014). On the basis of these evidences, we hypothesised that GA and T may be  
74 efficient candidates for inhibiting bacterial infections. Thus we developed a series of novel

75 bio-composites *e.g.*, GA-*g*-P(3HB)-*g*-EC and T-*g*-P(3HB)-*g*-EC and investigated their  
76 biocompatibility and antibacterial activity *in-vitro* against human keratinocytes-like cell, and  
77 Gram-positive and Gram-negative bacterial strains respectively.

78

## 79 **2. Materials and Methods**

80

### 81 **2.1. Chemicals**

82 Dulbecco's modified eagle's medium (DMEM), phosphate buffer saline (PBS), streptomycin  
83 and was penicillin were obtained from Lonza, UK. Fetal calf serum was received from  
84 Labtech International Ltd., UK. Table 1 illustrates physiochemical characteristics of GA and  
85 T obtained from Sigma-Aldrich Company Ltd., UK.

86

### 87 **2.2. Microorganisms**

88 *B. subtilis* NCTC 3610, *S. aureus* NCTC 6571, *E. coli* NTCT 10418 and *P. aeruginosa*  
89 NCTC 10662 strains were obtained from the culture collection unit of the University of  
90 Westminster London, UK. An overnight grown inoculum of each of the aforementioned  
91 strains was developed, separately, in 50 mL sterile nutrient broth under temperature  
92 controlled environment at 30 °C and 120 rpm.

93

### 94 **2.3. Grafting of phenols onto P(3HB)-*g*-EC**

95 The grafting of GA and T onto the previously developed P(3HB)-*g*-EC composite (Iqbal et  
96 al., 2014b), was performed via surface dipping and incorporation technique. A pre-weight  
97 P(3HB)-*g*-EC was dipped in a 50 mL solution of GA and T, separately. Control sample,  
98 [P(3HB)-*g*-EC], was treated with buffer alone without GA and/or T. After the stipulated  
99 reaction time (60 min), the weight of each composite was recorded followed by incubation at

100 50 °C until fully dried and final dry weight was recorded. The dried films were designated as  
101 GA-g-P(3HB)-g-EC bio-composites *i.e.*, [0GA-g-P(3HB)-g-EC (control); 5GA-g-P(3HB)-g-  
102 EC; 10GA-g-P(3HB)-g-EC; 15GA-g-P(3HB)-g-EC and 20GA-g-P(3HB)-g-EC] and T-g-  
103 P(3HB)-g-EC bio-composites *i.e.*, [0T-g-P(3HB)-g-EC (control); 5T-g-P(3HB)-g-EC; 10T-g-  
104 P(3HB)-g-EC; 15T-g-P(3HB)-g-EC and 20T-g-P(3HB)-g-EC] and used as prepared for  
105 further evaluation.

106

#### 107 **2.4. Fourier Transform Infrared spectroscopy (FT-IR)**

108 The individual and grafted composites were placed on the diamond crystal, and infrared  
109 absorption spectra were recorded from the wavelength region of 4000-500 cm<sup>-1</sup> using a  
110 Perkin Elmer System 2000 FT-IR spectrophotometer. All spectra were collected with 64  
111 scans and 2 cm<sup>-1</sup> resolution and assigned peak numbers.

112

#### 113 **2.5. Grafting parameters**

114 The grafting parameters *i.e.*, graft yield (GY %), grafting efficiency (GE %) and swelling  
115 ratio (SR %) behaviours of the GA-g-P(3HB)-g-EC and T-g-P(3HB)-g-EC bio-composites  
116 were investigated. The aforementioned parameters were calculated according to the following  
117 equations with minor modifications as reported earlier by Sabaa et al., 2012.

$$118 \quad \text{Graft yield (GY\%)} = [(W_f - W_i) / W_i] \times 100 \quad (1)$$

$$119 \quad \text{Grafting efficiency (GE\%)} = [(W_f - W_i) / (W_s - W_i)] \times 100 \quad (2)$$

$$120 \quad \text{Swelling ratio (SR\%)} = (W_s - W_i) / W_i \times 100 \quad (3)$$

121 *Where, W<sub>i</sub> = initial weight before immersion; W<sub>f</sub> = final dry weight after immersion; and W<sub>s</sub>*  
122 *= weight of sample at the swollen state*

123

#### 124 **2.6. Antibacterial activity assay**

125 The antibacterial activities of GA-g-P(3HB)-g-EC and T-g-P(3HB)-g-EC bio-composites  
 126 were inspected against Gram-positive (*B. subtilis* NCTC 3610 and *S. aureus* NCTC 6571)  
 127 and Gram-negative (*E. coli* NTCT 10418 and *P. aeruginosa* NCTC 10662) strains. An  
 128 overnight grown spore suspensions of each bacteria were inoculated on the pre-sterilised  
 129 surfaces of GA-g-P(3HB)-g-EC and T-g-P(3HB)-g-EC bio-composites, followed by  
 130 incubation in a temperature controlled incubator at 30 °C for 24 h. After the stipulated  
 131 incubation time period (24 h), the bacterial cells were washed twice using 50 mL phosphate  
 132 buffer (pH, 7.0) and the viable cells were calculated as CFU/mL by conventional spread-plate  
 133 method by serial dilution. In comparison to control (initial bacterial count *i.e.*, 10<sup>5</sup> CFU/mL),  
 134 the mean colony forming units per mL (CFU/mL) values were used to calculate the reduction  
 135 in log value by using the Equation 4.

$$\text{Log reduction} = \log \text{CFU control sample} - \log \text{CFU treated sample} \quad (4)$$

### 138 **2.7. *In-vitro* cell viability assay**

139 To evaluate the cytotoxicity of the newly synthesised GA-g-P(3HB)-g-EC and T-g-P(3HB)-  
 140 g-EC bio-composites a human keratinocytes-like HaCaT cell line was adopted, in this study.  
 141 HaCaT cell viability was measured after 1, 3 and 5 days of incubation using neutral red assay  
 142 as reported earlier (Iqbal et al., 2015). The HaCaT cell viability in percentage was calculated  
 143 using the Equation 5. Whereas, the adherent morphology of HaCaT cells seeded on the  
 144 P(3HB)-g-EC, GA-g-P(3HB)-g-EC and T-g-P(3HB)-g-EC bio-composites was observed  
 145 using Nikon light microscope. After 1 h incubation in neutral red dye solution, the stained  
 146 cells were washed with PBS prior to record images at 100× magnification.

$$\% \text{ cell viability} = \frac{\text{OD}_{\text{Test specimen}} - \text{OD}_{\text{Negative control}}}{\text{OD}_{\text{Positive control}}} \times 100 \quad (5)$$



150 *Standard tissue culture plastic was used as a positive control whereas graft composite*  
151 *without cell culture was used as negative control to normalise the absorption of the neutral*  
152 *red dye by the graft composite itself.*

153

## 154 **2.8. Soil Burial Test**

155 The biodegradability of GA-g-P(3HB)-g-EC and T-g-P(3HB)-g-EC bio-composites was  
156 evaluated using soil burial test as-described earlier by Wattanakornsiri et al., 2012. After  
157 every 7 days of burial, each set was removed, washed, dried and subsequently weighed to  
158 determine the loss in weight, being recorded every week for 6 weeks. The percentage of  
159 weight loss was calculated using the Equation 6.

$$\begin{aligned} & \text{Control weight} - \text{loss in weight} \\ \text{\% Loss in weight} = & \frac{\text{Control weight} - \text{loss in weight}}{\text{Control weight}} \times 100 \end{aligned} \quad (6)$$

163

## 164 **3. Results and Discussion**

165 The FT-IR spectra were used to characterise the structural elements of GA, T, P(3HB)-g-EC,  
166 GA-g-P(3HB)-g-EC and T-g-P(3HB)-g-EC (shown in Figure 2A and B). For GA-g-P(3HB)-  
167 g-EC, the absorptions at 3345, 1720, 1360, and 1056  $\text{cm}^{-1}$  in the spectrum are indications of  
168 GA. The region between 1260 and 1056  $\text{cm}^{-1}$  relates to the C–H and C–O–C bond stretching  
169 frequencies; a band at 2985  $\text{cm}^{-1}$  is assigned to C–H vibration; the band range from 3200 to  
170 3400  $\text{cm}^{-1}$  corresponds to the vibration stretching of inter- and intramolecular hydrogen bonds  
171 of GA-g-P(3HB)-g-EC. The peak at 1000–1150  $\text{cm}^{-1}$ , corresponding mainly to ethers (C–O–  
172 C), increased compared to phenolics monomers spectra, indicating extended polymerisation  
173 (Yamada et al., 2007). It has typical polyphenol characteristics, showing broad peaks centred  
174 at 3345 and 1375  $\text{cm}^{-1}$  due to the vibration of O–H linkage of phenolic and hydroxyl groups,  
175 at 1450–1600  $\text{cm}^{-1}$  due to the aromatic ring C=C stretching, and C=O stretching vibration at  
176 1200–1300  $\text{cm}^{-1}$ , respectively. A new peak at 1625  $\text{cm}^{-1}$  is probably due to the quinone

177 moiety absorption. The most intense peaks at 738 and 807  $\text{cm}^{-1}$  are assigned to ring vibrations  
178 of the T chemistry (Schulz et al., 2003; Torres-Giner et al., 2014). Figure 2B depict an  
179 increase in the hydrogen bond peak at 3360  $\text{cm}^{-1}$  as a result of T affinity to the P(3HB)-g-EC,  
180 this peak was not found in the spectra of pristine T. The T-g-P(3HB)-g-EC spectra exhibit a  
181 different profile compared to the spectra of pure T alone. The bands in the 3070–2860  $\text{cm}^{-1}$   
182 region are assigned to the C–H,  $\text{CH}_2$  and  $\text{CH}_3$  vibrations. In the fingerprint region, there are  
183 bands assigned to the aromatic and hetero aliphatic rings as well as to the  $\text{CH}_2$  and  $\text{CH}_3$   
184 modes. The peak at 1000–1150  $\text{cm}^{-1}$ , corresponding mainly to C-O-C linkages, increased  
185 compared to phenolics monomers spectra, indicating extended polymerisation (Yamada et al.,  
186 2007; Božič et al., 2012). By comparison between this and the T-g-P(3HB)-g-EC spectra, it  
187 can be seen that some bands changed intensity and/or shape during the graft formation  
188 process.

189

190 Figs. 3 A and B shows the graft yield (GY%), grafting efficiency (GE%) and swelling ratio  
191 (SR%) profiles of GA-g-P(3HB)-g-EC *i.e.*, 0GA-g-P(3HB)-g-EC, 5GA-g-P(3HB)-g-EC,  
192 10GA-g-P(3HB)-g-EC, 15GA-g-P(3HB)-g-EC and 20GA-g-P(3HB)-g-EC and T-g-P(3HB)-  
193 g-EC *i.e.*, 0T-g-P(3HB)-g-EC, 5T-g-P(3HB)-g-EC, 10T-g-P(3HB)-g-EC, 15T-g-P(3HB)-g-  
194 EC and 20T-g-P(3HB)-g-EC bio-composites. A consistent increase in all of the grafting  
195 parameters *i.e.*, GY%, GE% and SR% was recorded up to the concentration of 15 mM GA,  
196 whereas, in case of T 20 mM concentration was proved best under the same environment.  
197 However, further increase up to 20 mM GA concentration showed decreasing trend in  
198 aforementioned parameters. One possible reason for the observed behaviour could be the  
199 substantial amount of GA grafted onto the P(3HB)-g-EC bio-composite, which creates steric  
200 hindrance for further grafting. The increase in monomer concentration would be expected to  
201 increase both the grafting percentage which in turn increase the molecular weight of the graft

202 composite (Aggour, 2001; Constantin et al., 2011). Indeed, the results presented in Figure 3  
203 indicate that as the concentration of GA increases from 0 to 15 mM both the GY% and GE%  
204 were optimal with an increase in the swelling ratio. The order of GP % observed for GA-g-  
205 P(3HB)-g-EC and T-g-P(3HB)-g-EC composites was: 15GA-g-P(3HB)-g-EC > 10GA-g-  
206 P(3HB)-g-EC > 20GA-g-P(3HB)-g-EC > 5GA-g-P(3HB)-g-EC > 0GA-g-P(3HB)-g-EC and  
207 20T-g-P(3HB)-g-EC > 15T-g-P(3HB)-g-EC > 10T-g-P(3HB)-g-EC > 5T-g-P(3HB)-g-EC >  
208 0T-g-P(3HB)-g-EC respectively. It has also been reported in literature that the reaction time  
209 is an important parameter which can increase or decrease the grafting parameters like graft  
210 yield, grafting efficiency and swelling behaviour (Sun et al., 2003; Constantin et al., 2011).

211

212 The results of the disc diffusion method for GA-g-P(3HB)-g-EC bio-composites against each  
213 bacterial strain are given in the Fig. 4 (A-D). 0GA-g-P(3HB)-g-EC used as a control, did not  
214 showed any log reduction (CFU/mL) against *B. subtilis* NCTC 3610, *S. aureus* NCTC 6571,  
215 *E. coli* NTCT 10418 and *P. aeruginosa* NCTC 10662, thus showing no antibacterial  
216 potentials. 5GA-g-P(3HB)-g-EC and 20GA-g-P(3HB)-g-EC composites prepared with 5 and  
217 20 mM GA concentration, respectively, did not show any potential to inhibit bacterial count  
218 against each of the above said bacterial species. However, the composite prepared by the  
219 incorporation of 10 and 15 mM GA onto P(3HB)-g-EC backbone material displayed  
220 excellent antibacterial activities against all of the tested species (Fig. 4, A-D). For the  
221 samples prepared in the presence of laccase, the results clearly show that increasing the  
222 concentration of T the antibacterial activity is enhanced, reaching a complete bactericidal  
223 effect at 20 mM concentration against test microorganisms. As already seen in Fig. 5 (A-D),  
224 the bio-composites, prepared with varying T concentrations (0 to 20 mM) in the presence of  
225 laccase, produced a slight bacteriostatic effect on *B. subtilis* NCTC 3610 and *S. aureus*  
226 NCTC 6571, in the range 15 and 20 mM concentration. The same composites with the same

227 concentration showed complete bactericidal effect on *E. coli* NTCT 10418 and *P. aeruginosa*  
228 NCTC 10662. The counting test showed a complete bactericidal effect (100 % reduction of  
229 bacterial count) on *E. coli* NTCT 10418 and *S. aureus* NCTC 6571, but only in the case of  
230 graft composites prepared with 15 mM and 20 mM T concentrations. This is because the  
231 interaction between T and bacteria can change the metabolic activity of bacteria and  
232 eventually cause their death. However, the exact mechanism of the antimicrobial action of T  
233 is not established yet. Based on an earlier publication, T has an ability to disrupt the lipid  
234 structure of the bacterial cell wall leading to the destruction of the cell membrane,  
235 cytoplasmic leakage, and cell lysis and ultimately, cell death (Veras et al. 2012; Milovanovic  
236 et al., 2013; Shahidi et al., 2014).

237

238 Cell viability at 1, 3 and 5 days after seeding of HaCaT cells on the GA-g-P(3HB)-g-EC and  
239 T-g-P(3HB)-g-EC bio-composites, in comparison to those on the tissue culture plastic  
240 (polystyrene), are shown in Fig. 6 (A-F). The GA and T grafted bio-composites supported  
241 variable viability of HaCaT cells. The % viability of HaCaT cells at 5 days of incubation on  
242 GA and T grafted bio-composites were in the following order: 10GA-g-P(3HB)-g-EC >  
243 15GA-g-P(3HB)-g-EC > 5GA-g-P(3HB)-g-EC > 20GA-g-P(3HB)-g-EC > 0GA-g-P(3HB)-g-  
244 EC, and 15T-g-P(3HB)-g-EC > 20T-g-P(3HB)-g-EC > 10T-g-P(3HB)-g-EC > 5T-g-P(3HB)-  
245 g-EC > 0T-g-P(3HB)-g-EC. The Morphology of HaCaT cells grown on the GA-g-P(3HB)-g-  
246 EC and T-g-P(3HB)-g-EC bio-composites at 1, 3 and 5 days of seeding is shown in Figs. 7  
247 and 8, respectively. HaCaT cells responded to the test composites by exhibiting good  
248 attachment and spreading. Moreover, the growing HaCaT cells demonstrated normal cell  
249 morphology with their typical shape and spread covering the material surface.

250

251 Figs. 9 and 10 shows the degradation profiles of the GA-*g*-P(3HB)-*g*-EC composites and T-*g*-  
252 P(3HB)-*g*-EC composites after 6 weeks of soil burial degradation, respectively. Owing to the  
253 difficulty in isolating degraded part of the test samples from soil particles, the weight loss of  
254 composites induced by biodegradation in soil was recorded. Figs. 9 and 10 illustrate the %  
255 weight loss of the test composites as a function of degradation time. All of the composites  
256 showed an increased degradation rate to different extents during the burial period. In contrast  
257 to the results obtained with the soil burial test, a significant difference was revealed in this  
258 experiment with respect to degradation rate. It was observed that the degradation rate of the  
259 pristine P(3HB)-*g*-EC was lower than that of the GA and/or T incorporated GA-*g*-P(3HB)-*g*-  
260 EC and T-*g*-P(3HB)-*g*-EC bio-composites. After 6 weeks of incubation, up to 100% bio-  
261 degradability of GA-*g*-P(3HB)-*g*-EC and T-*g*-P(3HB)-*g*-EC bio-composites was recorded in  
262 comparison to the control sample. Mostly, the cellulosic based composites/blends can be  
263 degraded by a wide spectrum of cellulolytic or ligninolytic enzymes secreted by the soil  
264 bacteria or fungi. For example brown rot fungi are more effective in decomposing cellulose  
265 and hemicelluloses like components, whereas, white rot fungi are able to degrade phenol  
266 containing structures like lignin. Moreover, such natural process factually simulates the  
267 degradation situation when the used composites are abandoned as garbage.

268

#### 269 **4. Conclusions**

270 In conclusion, we prepared a series of novel bio-composites with natural phenols as  
271 functional entities which displayed an excellent antibacterial activity against Gram-positive  
272 and Gram-negative bacterial strains. The improved bacterial resistance along with human  
273 keratinocytes-like HaCaT compatibility indicate that the newly synthesised GA-*g*-P(3HB)-*g*-  
274 EC and T-*g*-P(3HB)-*g*-EC bio-composites are promising candidates for biomedical type  
275 applications such as skin regeneration, multiphasic tissue engineering and/or medical

276 implants. However further studies, especially *in-vivo* experiments are required for detailed  
277 information for other applications such as biomedical implants of these newly developed bio-  
278 composites.

279

## 280 **Acknowledgements**

281 This work was supported by the Cavendish Research Scholarship program of the University  
282 of Westminster London UK, a specialised research fund for the Doctoral Program for the  
283 University of Westminster Scholars.

284

## 285 **References**

286 Aggour, Y. A. (2001). Reaction kinetics of graft copolymerization and thermochemical  
287 studies of the degradation of poly(vinyl alcohol) graft copolymer. *Polymer*  
288 *International*, 50, 347-353.

289 Albers, C. E., Hofstetter, W., Siebenrock, K. A., Landmann, R., & Klenke, F. M. (2013). In  
290 vitro cytotoxicity of silver nanoparticles on osteoblasts and osteoclasts at antibacterial  
291 concentrations. *Nanotoxicology*, 7(1), 30-36.

292 Aljawish, A., Chevalot, I., Piffaut, B., Rondeau-Mouro, C., Girardin, M., Jasniewski, J., &  
293 Muniglia, L. (2012). Functionalization of chitosan by laccase-catalyzed oxidation of  
294 ferulic acid and ethyl ferulate under heterogeneous reaction conditions. *Carbohydrate*  
295 *Polymers*, 87(1), 537-544.

296 Archana, P. R., Rao, B. N., & Rao, B. S. (2011). Modulation of gamma ray-induced  
297 genotoxic effect by thymol, a monoterpene phenol derivative of cymene. *Integrative*  
298 *Cancer Therapies*, 10(4), 374-383.

299 Božič, M., Gorgieva, S., & Kokol, V. (2012). Homogeneous and heterogeneous methods for  
300 laccase-mediated functionalization of chitosan by tannic acid and  
301 quercetin. *Carbohydrate Polymers*, *89*(3), 854-864.

302 Chen, T., Kumar, G., Harris, M. T., Smith, P. J., & Payne, G. F. (2000). Enzymatic grafting  
303 of hexyloxyphenol onto chitosan to alter surface and rheological properties.  
304 *Biotechnology and Bioengineering*, *70*(5), 564-573.

305 Constantin, M., Mihalcea, I., Oanea, I., Harabagiu, V., & Fundueanu, G. (2011). Studies on  
306 graft copolymerization of 3-acrylamidopropyl trimethyl ammonium chloride on  
307 pullulan. *Carbohydrate Polymers*, *84*(3), 926-932.

308 Dong, C., Ye, Y., Qian, L., Zhao, G., He, B., & Xiao, H. (2014). Antibacterial modification  
309 of cellulose fibers by grafting  $\beta$ -cyclodextrin and inclusion with ciprofloxacin.  
310 *Cellulose*, *21*(3), 1921-1932.

311 Hiriart-Ramírez, E., Contreras-García, A., García-Fernández, M. J., Concheiro, A., Álvarez-  
312 Lorenzo, C., Bucio, E. (2012). Radiation grafting of glycidyl methacrylate onto cotton  
313 gauzes for functionalization with cyclodextrins and elution of antimicrobial agents.  
314 *Cellulose*, *19*(6), 2165-2177.

315 Iqbal, H. M. N., Kyazze, G., Locke, I. C., Tron, T., & Keshavarz, T. (2015). *In-situ*  
316 development of self-defensive antibacterial biomaterials: phenol-g-keratin-EC based  
317 bio-composites with characteristics for biomedical applications. *Green Chemistry*, In-  
318 Press, DOI: 10.1039/C5GC00715A.

319 Iqbal, H. M. N., Kyazze, G., Tron, T., & Keshavarz, T. (2014a). Laccase-assisted grafting of  
320 poly (3-hydroxybutyrate) onto the bacterial cellulose as backbone polymer:  
321 Development and characterisation. *Carbohydrate polymers*, *113*, 131-137.

322 Iqbal, H. M. N., Kyazze, G., Tron, T., & Keshavarz, T. (2014b). A preliminary study on the  
323 development and characterisation of enzymatically grafted P (3HB)-ethyl cellulose  
324 based novel composites. *Cellulose*, 21(5), 3613-3621.

325 Iqbal, H. M. N., Kyazze, G., Tron, T., & Keshavarz, T. (2014c). “One-pot” synthesis and  
326 characterisation of novel P (3HB)–ethyl cellulose based graft composites through lipase  
327 catalysed esterification. *Polymer Chemistry*, 5(24), 7004-7012.

328 Milovanovic, S., Stamenic, M., Markovic, D., Radetic, M., & Zizovic, I. (2013). Solubility of  
329 thymol in supercritical carbon dioxide and its impregnation on cotton gauze. *The*  
330 *Journal of Supercritical Fluids*, 84, 173-181.

331 Rukmani, A., & Sundrarajan, M. (2012). Inclusion of antibacterial agent thymol on  $\beta$ -  
332 cyclodextrin-grafted organic cotton. *Journal of Industrial Textiles*, 42(2), 132-144.

333 Sabaa, M. W., Mohamed, N. A., Mohamed, R. R., Khalil, N. M., & Abd El Latif, S. M.  
334 (2010). Synthesis, characterization and antimicrobial activity of poly (N-vinyl  
335 imidazole) grafted carboxymethyl chitosan. *Carbohydrate Polymers*, 79(4), 998-1005.

336 Sanchez-Garcia, M. D., Ocio, M. J., Gimenez, E., & Lagaron, J. M. (2008). Novel  
337 polycaprolactone nanocomposites containing thymol of interest in antimicrobial film  
338 and coating applications. *Journal of Plastic Film and Sheeting*, 24(3-4), 239-251.

339 Sandukas, S., Yamamoto, A., & Rabiei, A. (2011). Osteoblast adhesion to functionally  
340 graded hydroxyapatite coatings doped with silver. *Journal of Biomedical Materials*  
341 *Research Part A*, 97(4), 490-497.

342 Schulz, H., Quilitzsch, R., & Krüger, H. (2003). Rapid evaluation and quantitative analysis of  
343 thyme, origano and chamomile essential oils by ATR-IR and NIR spectroscopy.  
344 *Journal of Molecular Structure*, 661, 299-306.

345 Shahidi, S., Aslan, N., Ghoranneviss, M., & Korachi, M. (2014). Effect of thymol on the  
346 antibacterial efficiency of plasma-treated cotton fabric. *Cellulose*, 21(3), 1933-1943.



347 Sun, T., Xu, P., Liu, Q., Xue, J., & Xie, W. (2003). Graft copolymerization of methacrylic acid  
348 onto carboxymethyl chitosan. *European Polymer Journal*, 39, 189-192.

349 Torres-Giner, S., Martinez-Abad, A., & Lagaron, J. M. (2014). Zein-based ultrathin fibers  
350 containing ceramic nanofillers obtained by electrospinning. II. Mechanical properties,  
351 gas barrier, and sustained release capacity of biocide thymol in multilayer polylactide  
352 films. *Journal of Applied Polymer Science*. 131, 40768.

353 Veras, H. N., Rodrigues, F. F., Colares, A. V., Menezes, I. R., Coutinho, H. D., Botelho, M.  
354 A., & Costa, J. G. (2012). Synergistic antibiotic activity of volatile compounds from the  
355 essential oil of *Lippia sidoides* and thymol. *Fitoterapia*, 83(3), 508-512.

356 Wang, L., He, S., Wu, X., Liang, S., Mu, Z., Wei, J., Deng, F., deng, Y., & Wei, S. (2014).  
357 Polyetheretherketone/nano-fluorohydroxyapatite composite with antimicrobial activity  
358 and osseointegration properties. *Biomaterials*, 35, 6758-6775.

359 Wattanakornsiri, A., Pachana, K., Kaewpirom, S., Traina, M., & Migliaresi, C. (2012).  
360 Preparation and properties of green composites based on tapioca starch and differently  
361 recycled paper cellulose fibers. *Journal of Polymers and the Environment*, 20(3), 801-  
362 809.

363 Yamada, K., Abe, T., & Tanizawa, Y. (2007). Black tea stain formed on the surface of  
364 teacups and pots. Part 2—Study of the structure change caused by aging and calcium  
365 addition. *Food Chemistry*, 103, 8-14.

366 Yamada, K., Chen, T., Kumar, G., Vesnovsky, O., Topoleski, L. T., & Payne, G. F. (2000).  
367 Chitosan based water-resistant adhesive. Analogy to mussel glue. *Biomacromolecules*,  
368 1(2), 252-258.

369

370

371

372 **Figure captions**

373 **Figure 1** A tentative schematic representation of a proposed mechanism of graft formation  
374 through laccase-assisted grafting of gallic acid (as a model phenolic structure) onto the  
375 P(3HB)-g-EC based material. There are other possibilities too to depict the proposed  
376 mechanism of graft formation between phenol (used) and P(3HB)-g-EC based material.

377 **Figure 2** FT-IR spectra; (A) gallic acid (GA) and GA-g-P(3HB)-g-EC bio-composites and (B)  
378 thymol (T) and T-g-P(3HB)-g-EC bio-composites.

379 **Figure 3** Evaluation of grafting parameters *i.e.*, graft yield (GY %), grafting efficiency  
380 (GE %) and swelling ratio (SR %) behaviours of GA-g-P(3HB)-g-EC bio-composites (A) and  
381 T-g-P(3HB)-g-EC bio-composites (B).

382 **Figure 4** Antimicrobial activity of GA-g-P(3HB)-g-EC composites against *B. subtilis* NCTC  
383 3610 (A); *S. aureus* NCTC 6571 (B); *E. coli* NTCT 10418 (C) and *P. aeruginosa* NCTC  
384 10662 (D).

385 **Figure 5** Antimicrobial activity of T-g-P(3HB)-g-EC bio-composites against *B. subtilis*  
386 NCTC 3610 (A); *S. aureus* NCTC 6571 (B); *E. coli* NTCT 10418 (C) and *P. aeruginosa*  
387 NCTC 10662 (D).

388 **Figure 6** Neutral red dye concentration dependent percentage cell viability of HaCaT cells  
389 seeded on the GA-g-P(3HB)-g-EC bio-composites (A) 1 day; (B) 3 days and (C) 5 days; and  
390 HaCaT cells seeded on the T-g-P(3HB)-g-EC bio-composites (D) 1 day; (E) 3 days; (F) 5  
391 days.

392 **Figure 7** Adherent morphology of HaCaT cells seeded on the GA-g-P(3HB)-g-EC bio-  
393 composites. All of the test samples were stained using neutral red dye (5 mg/mL) for 1 h  
394 followed by three consecutive washings with PBS at an ambient temperature.

395 **Figure 8** Adherent morphology of HaCaT cells seeded on the T-g-P(3HB)-g-EC bio-  
396 composites. All of the test samples were stained using neutral red dye (5 mg/mL) for 1 h  
397 followed by three consecutive washings with PBS at an ambient temperature.

398 **Figure 9** Effect of soil burial period on the biodegradability of GA-g-P(3HB)-g-EC bio-  
399 composites *i.e.*, 0GA-g-P(3HB)-g-EC (□), 5GA-g-P(3HB)-g-EC (▤), 10GA-g-P(3HB)-g-  
400 EC (▥), 15GA-g-P(3HB)-g-EC (▦) and 20GA-g-P(3HB)-g-EC (■) buried for prescribed  
401 periods *i.e.*, (A) 7 days; (B) 14 days; (C) 21 days; (D) 28 days; (E) 35 days and (F) 42 days.

402 **Figure 10** Effect of soil burial period on the biodegradability of T-g-P(3HB)-g-EC bio-  
403 composites *i.e.*, 0T-g-P(3HB)-g-EC (□), 5T-g-P(3HB)-g-EC (▤), 10T-g-P(3HB)-g-EC (▥),  
404 15T-g-P(3HB)-g-EC (▦) and 20T-g-P(3HB)-g-EC (■) buried for prescribed periods *i.e.*, (A)  
405 7 days; (B) 14 days; (C) 21 days; (D) 28 days; (E) 35 days and (F) 42 days.

406

407

408

409

410

411

412

413

414

415

416

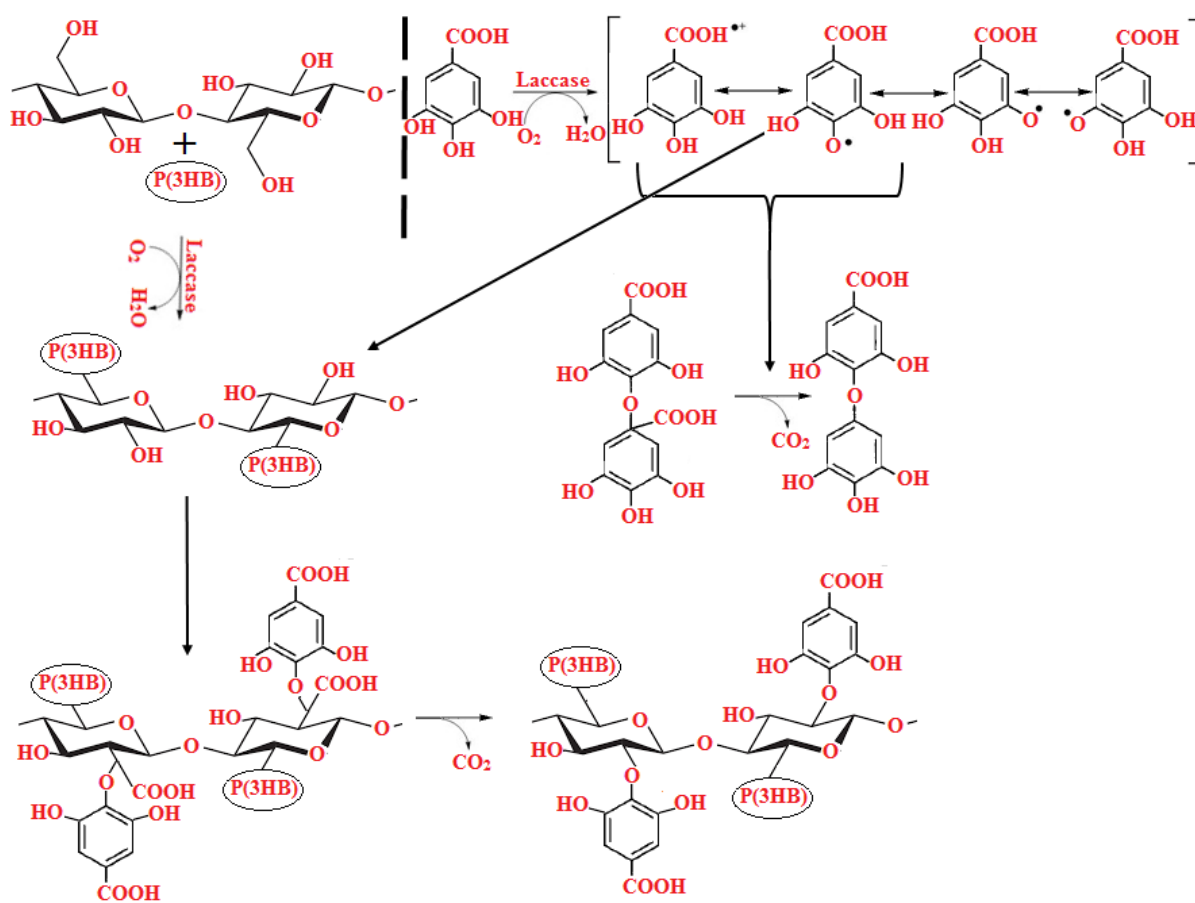
417

418

419

420 List of Figures

421 Figure 1



422

423

424

425

426

427

428

429

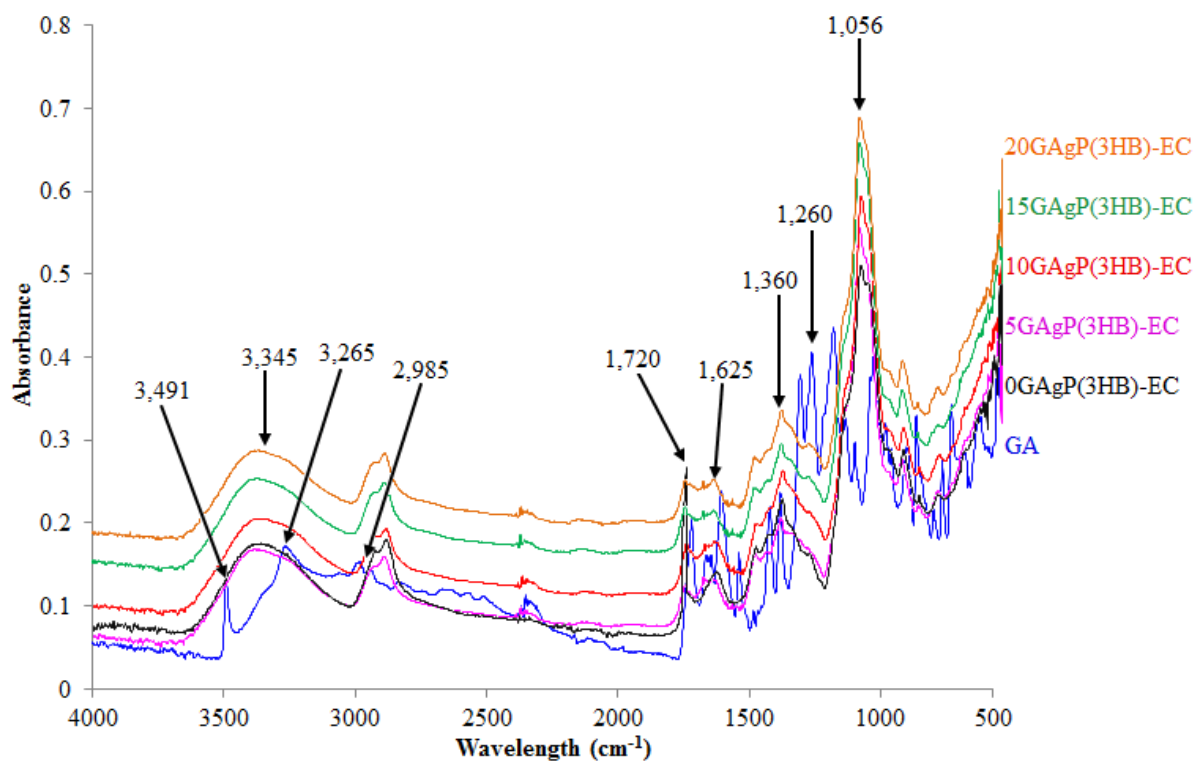
430

431

432

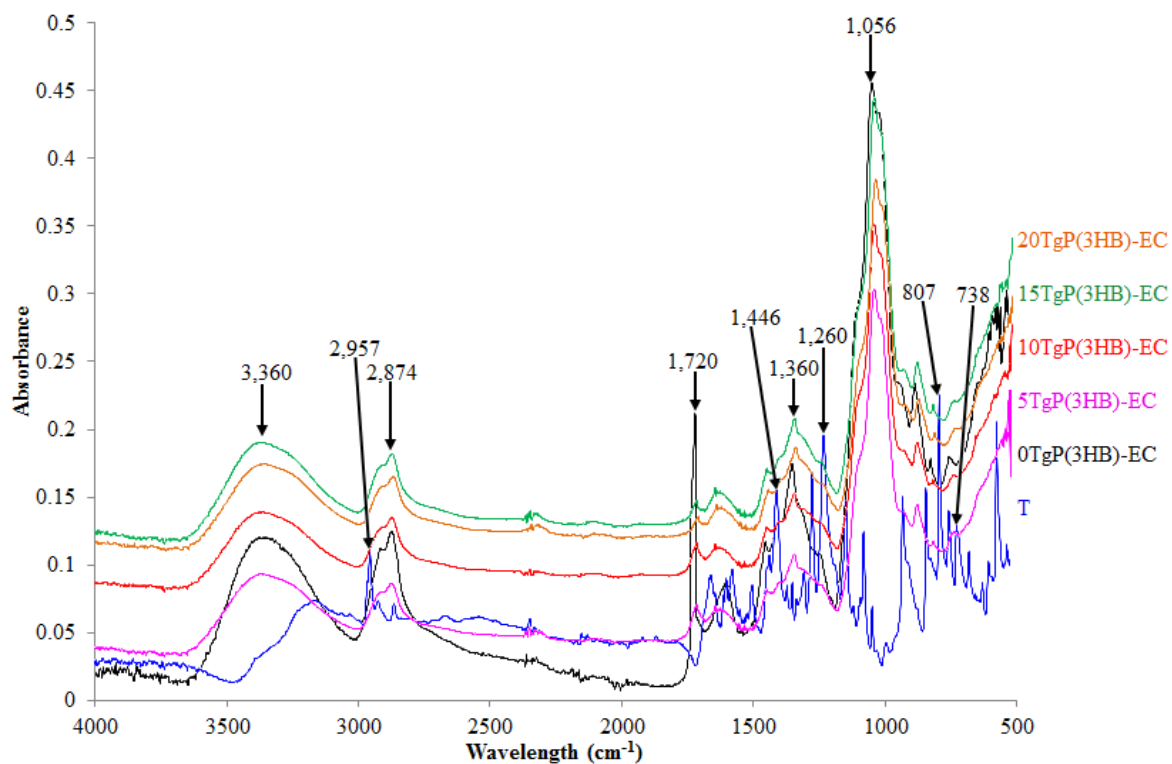
433

434 **Figure 2 A**



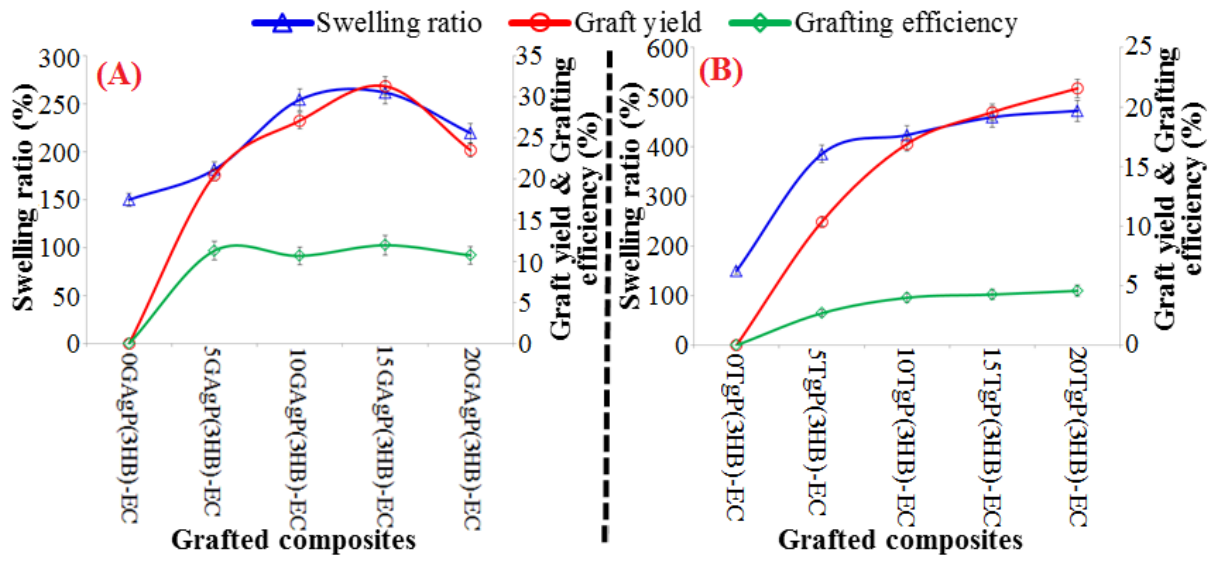
435  
436  
437  
438  
439  
440  
441  
442  
443  
444  
445  
446  
447  
448  
449

450 **Figure 2 B**



451  
452  
453  
454  
455  
456  
457  
458  
459  
460  
461  
462  
463  
464  
465

466 **Figure 3**



467

468

469

470

471

472

473

474

475

476

477

478

479

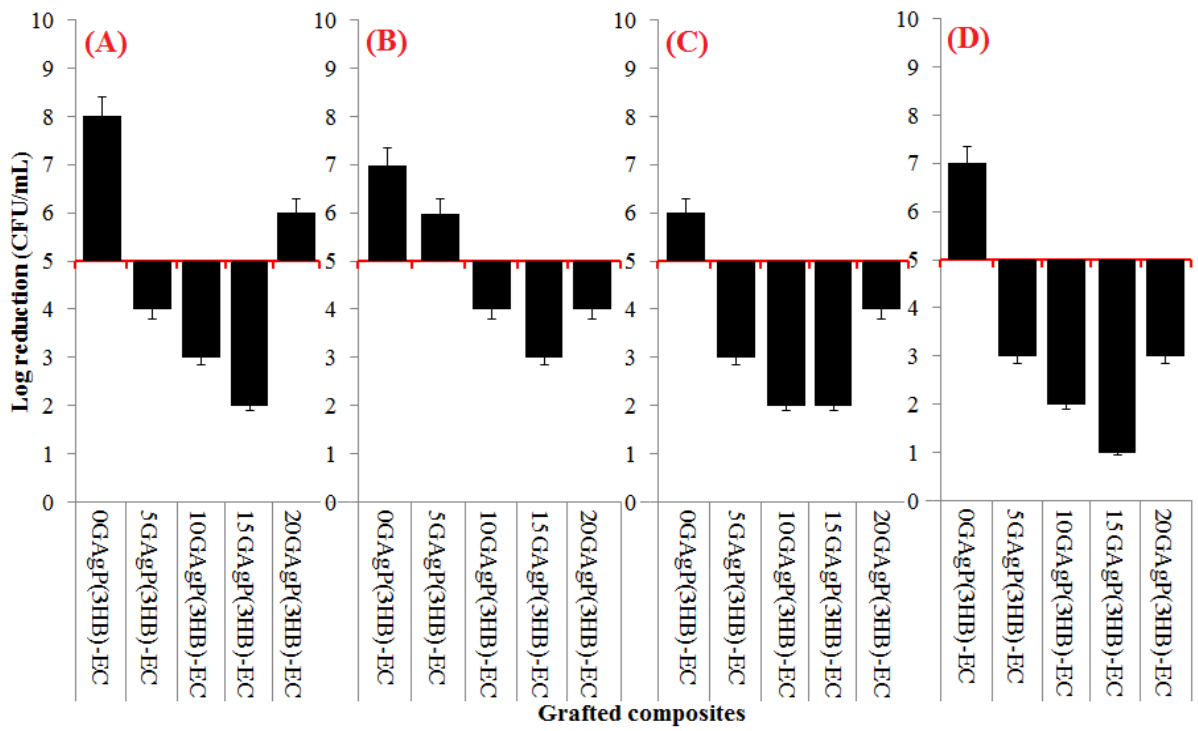
480

481

482

483

484 **Figure 4**



485

486

487

488

489

490

491

492

493

494

495

496

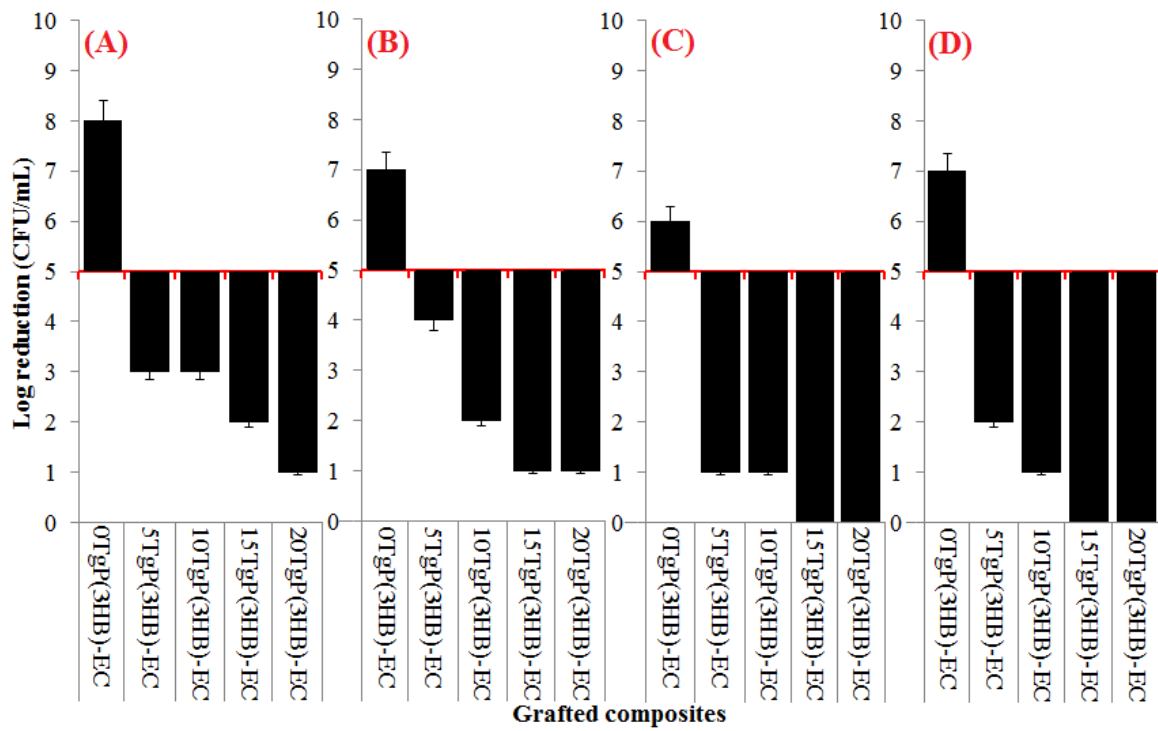
497

498

499



500 **Figure 5**



501

502

503

504

505

506

507

508

509

510

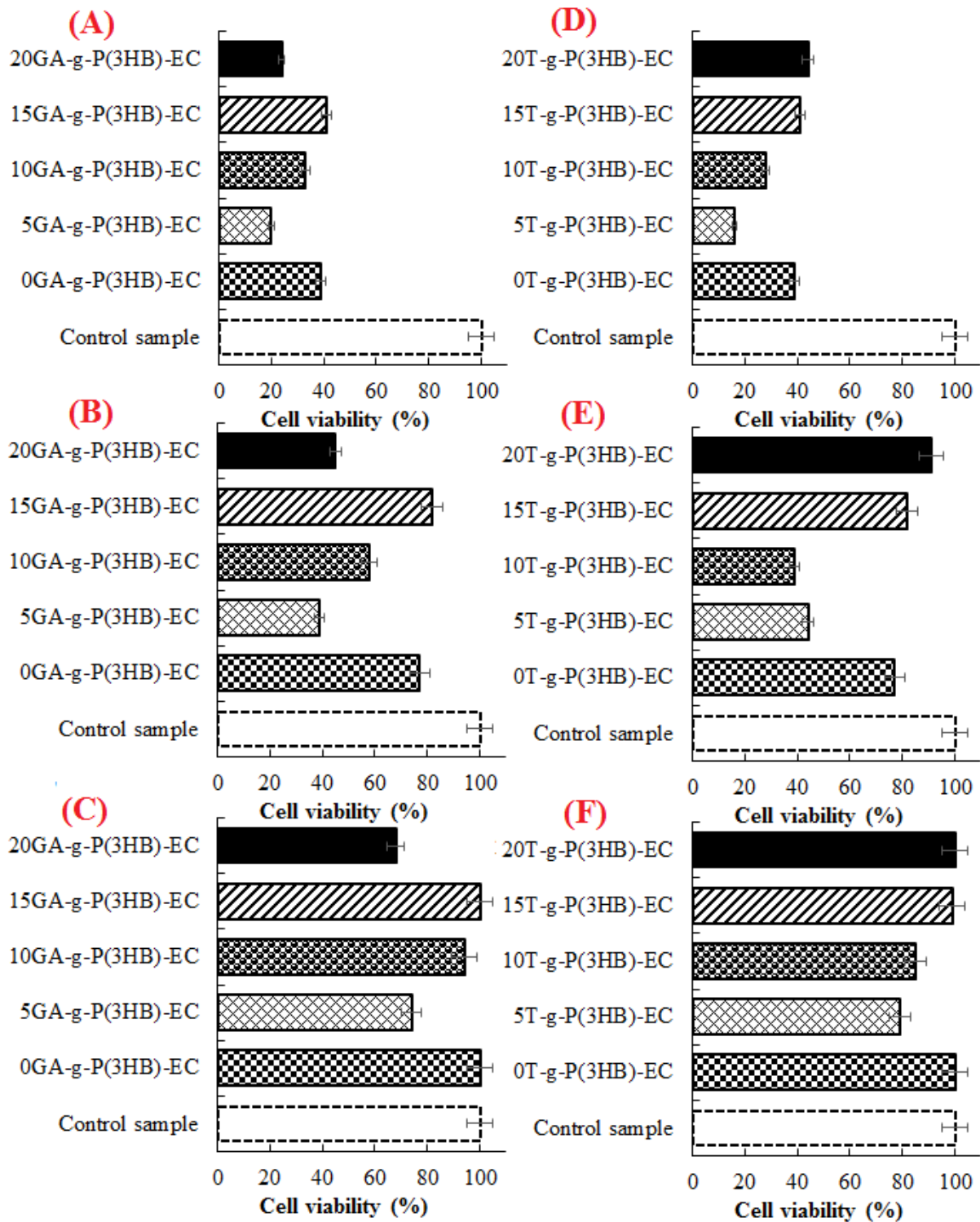
511

512

513

514

515



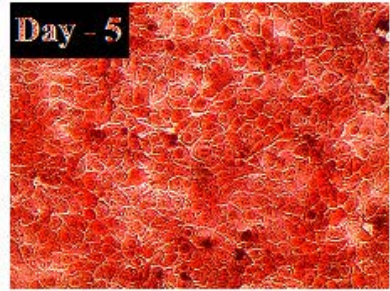
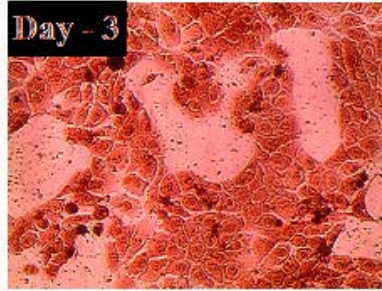
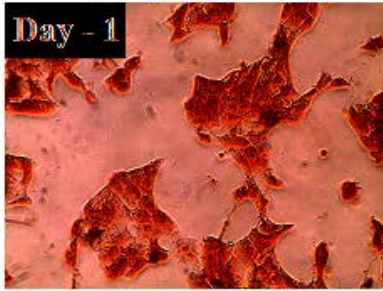
517

518

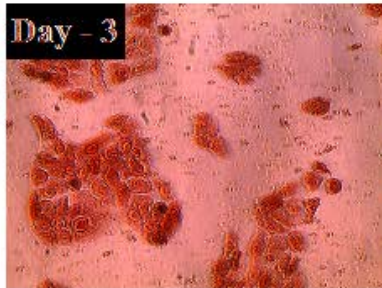
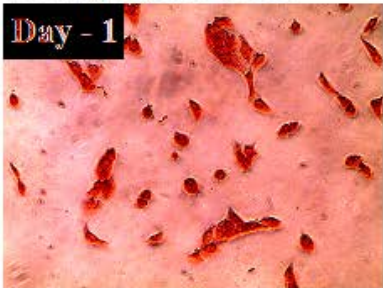
519

520

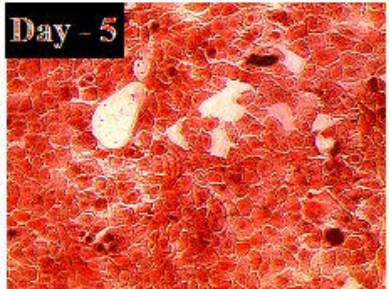
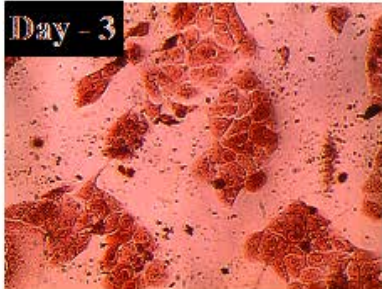
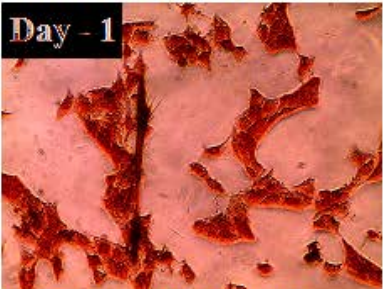
**0GA-g-P(3HB)-EC**



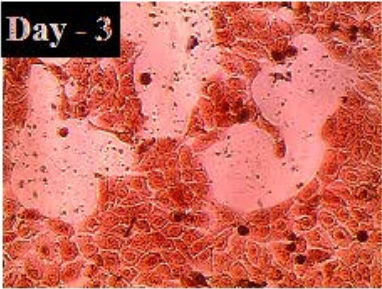
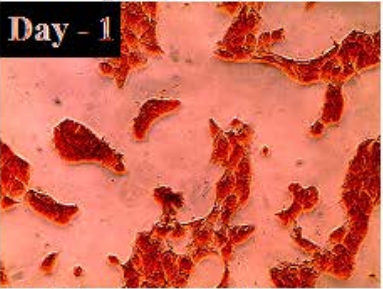
**5GA-g-P(3HB)-EC**



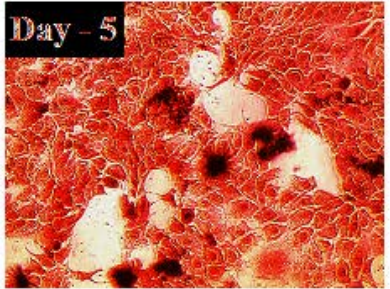
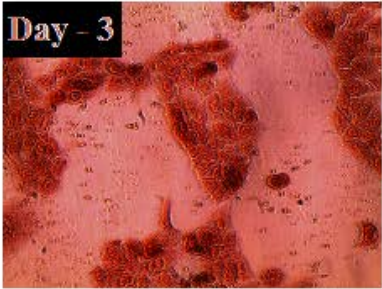
**10GA-g-P(3HB)-EC**



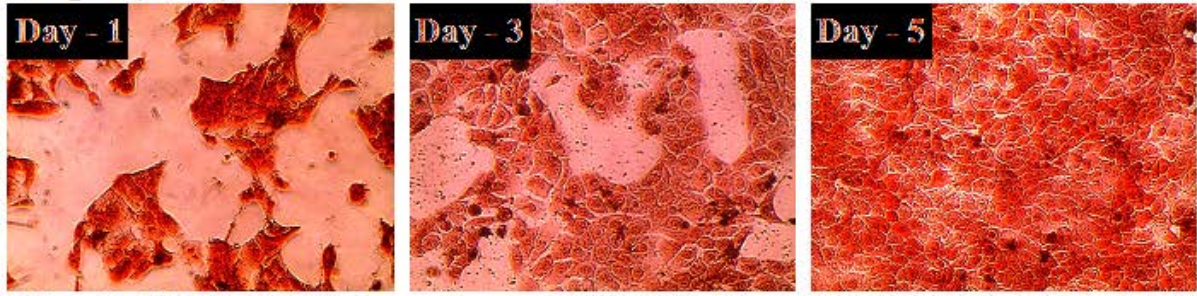
**15GA-g-P(3HB)-EC**



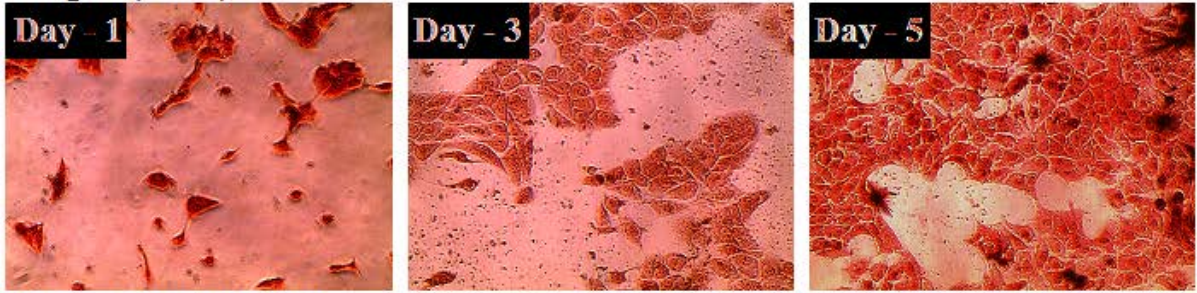
**20GA-g-P(3HB)-EC**



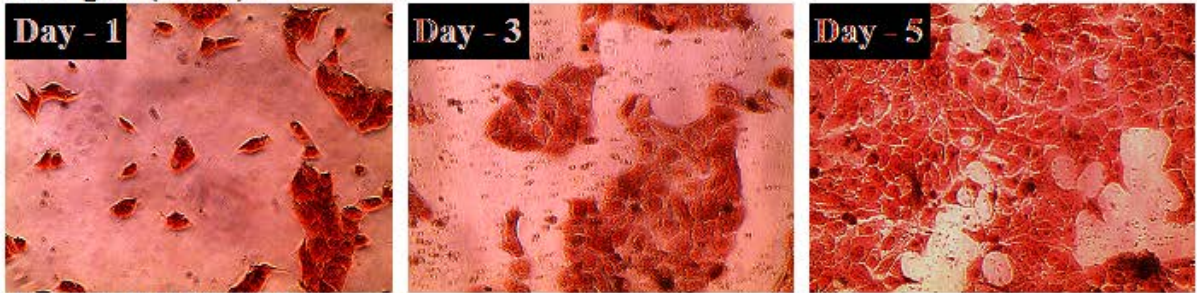
**0T-g-P(3HB)-EC**



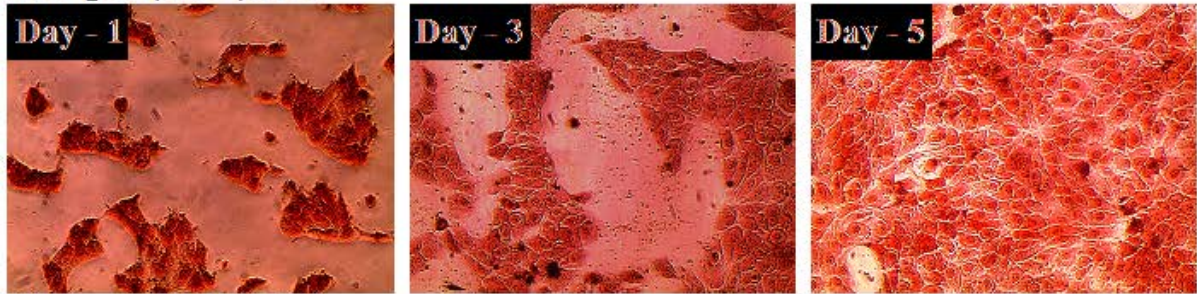
**5T-g-P(3HB)-EC**



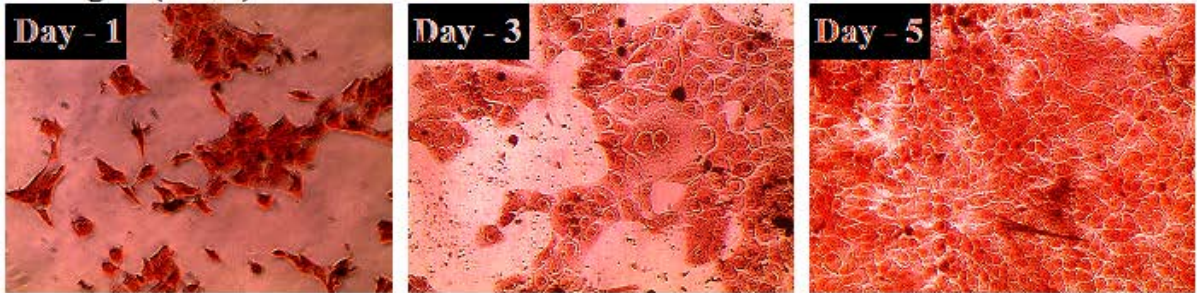
**10T-g-P(3HB)-EC**



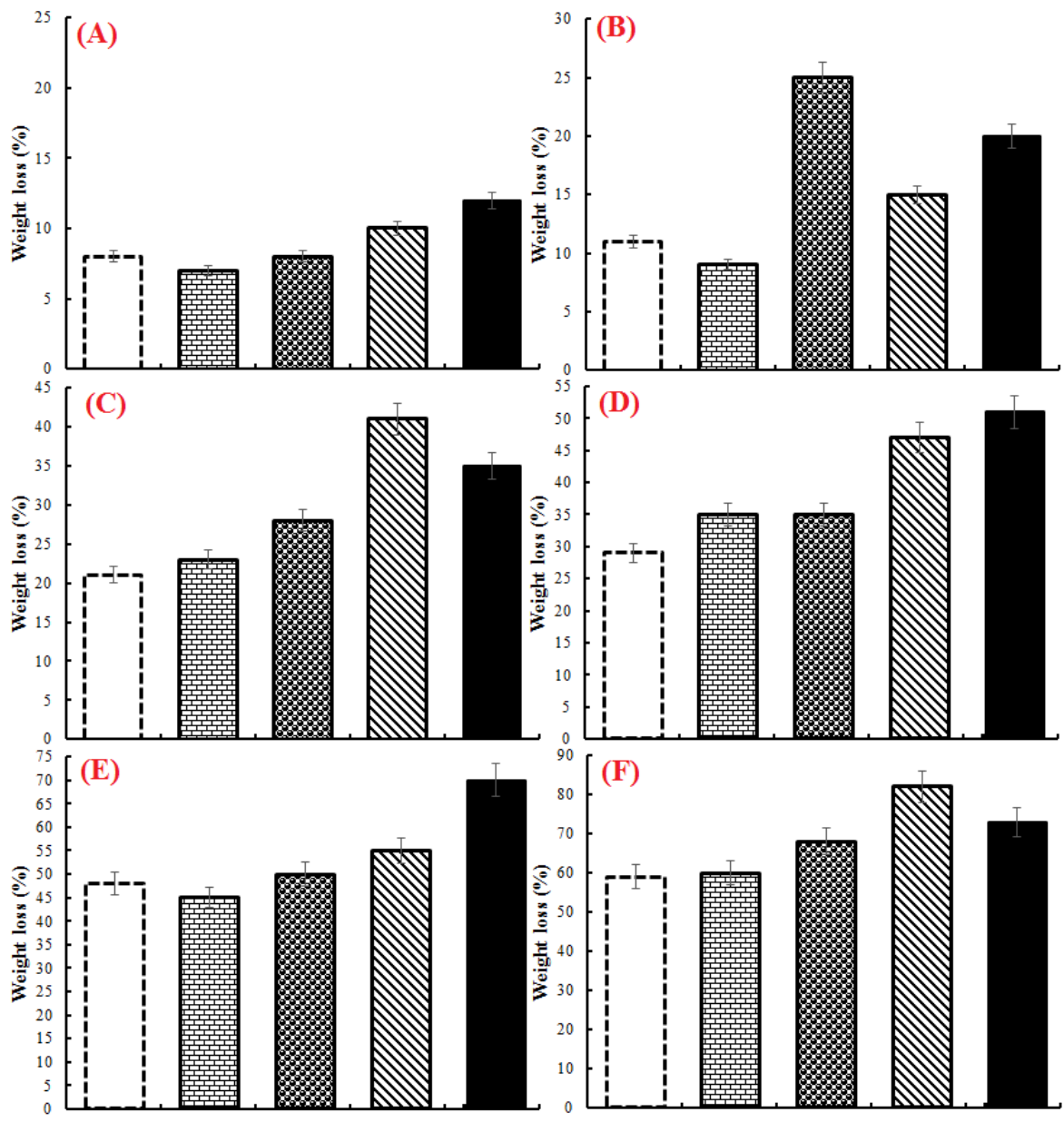
**15T-g-P(3HB)-EC**



**20T-g-P(3HB)-EC**



528 **Figure 9**



529

530

531

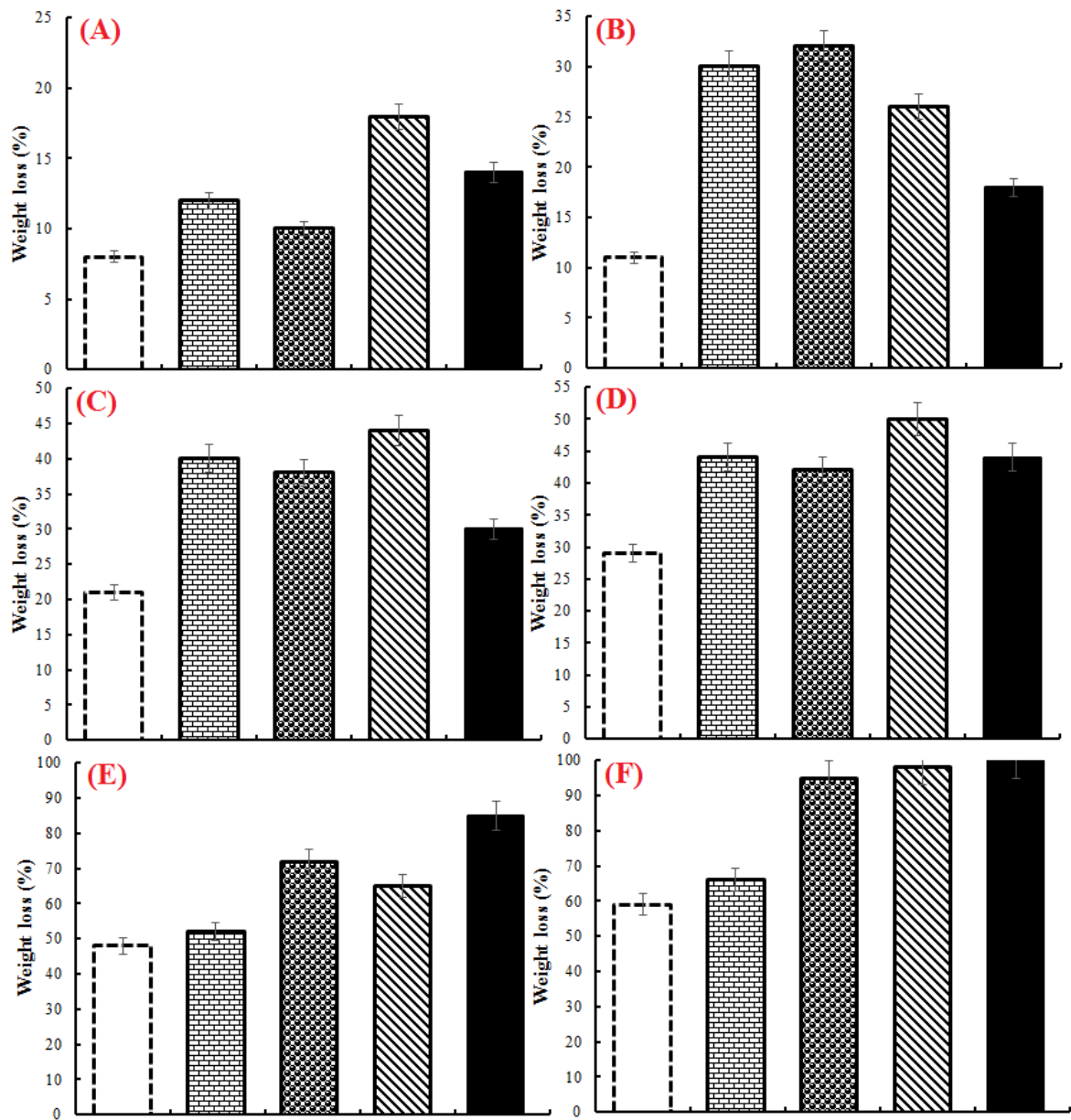
532

533

534

535

536



538

539

540

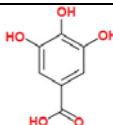
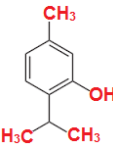
541

542

543

544

545 **Table 1** Physiochemical characteristics of the natural phenols used in this study for grafting  
 546 purposes.

Natural phenols	Appearance	Molecular formula	Molecular mass (g/mol)	Density (g/cm <sup>3</sup> )	Melting point (°C)	Functional groups	Structure
Gallic acid	White or yellow-white powder	C <sub>6</sub> H <sub>2</sub> (OH) <sub>3</sub> COOH	170.12	1.694	260	Hydroxyl and carboxylic	
Thymol	White crystalline	C <sub>10</sub> H <sub>14</sub> O	150.22	0.96	49-51	Hydroxyl	

547